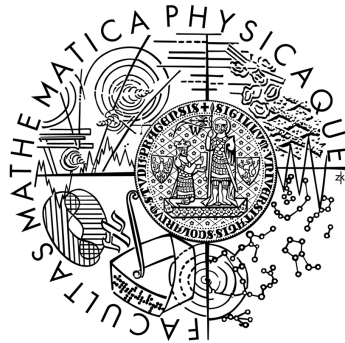Charles University in Prague

Faculty of Mathematics and Physics

MASTER THESIS

Lukáš Malina

Track measurement with the ATLAS Inner Detector

Institute of Particle and Nuclear Physics

Supervisor: Dr. Zdeněk Doležal

Study programme: Physics

Specialization: Nuclear and Subnuclear Physics

Prague 2014

I would like to express my gratitude to my supervisor Zdeněk Doležal for his valuable advices and help, especially with urgent matters. I would like to thank Andi Salzburger for the introduction into the tracking in dense environment, fruitful discussions and his enthusiastic approach. I also want to thank Zdeněk Hubáček for the proofreading and for his constructive criticism.

I declare that I carried out this master thesis independently, and only with the cited sources, literature and other professional sources.

I understand that my work relates to the rights and obligations under the Act No. 121/2000 Coll., the Copyright Act, as amended, in particular the fact that the Charles University in Prague has the right to conclude a license agreement on the use of this work as a school work pursuant to Section 60 paragraph 1 of the Copyright Act.

Geneva, 11th April 2014   Signature

Název práce: Měření drah částic pomocí vnitřního detektoru ATLAS

Autor: Lukáš Malina

Katedra: Ústav částicové a jaderné fyziky

Vedoucí diplomové práce: Doc. RNDr. Zdeněk Doležal, Dr., ÚČJF

Abstrakt: SCT je křemíkový stripový detektor, který je součástí vnitřního detektoru experimentu ATLAS na urychlovači LHC. Měření drah částic pomocí SCT je ovlivněno několika fundamentálními efekty: mnohonásobným rozptylem, Lorentzovým driftem, fluktuacemi energetických ztrát, zásahy způsobenými šumem a produkcí tzv. δ-elektronů. Tématem této diplomové práce je studie a korekce záření δ provedená na vyžádání skupiny detektoru SCT. Klastry, obsahující δ-elektrony, přiřazené drahám částic byly prozkoumány s využitím dat, která musela být za tímto účelem speciálně vytvořena. Zároveň byla úspěšně vyvinuta korekce pozic ovlivněných klastrů, která byla implementována do programového prostředí ATHENA určeného pro zpětnou rekonstrukci srážek. Funkčnost korekce v rámci rekonstrukce dat byla prostudována, její nadále probíhající detailní ověření však jde za rámec této práce. Vzhledem k četnosti a velikosti korekce bylo navrženo její použití k přesnějšímu měření pozice jednotlivých částí detektoru.

Klíčová slova: ATLAS, ATHENA, δ-elektron, křemíkový stripový detektor

Title: Track measurement with the ATLAS Inner Detector

Author: Lukáš Malina

Department: Institute of Particle and Nuclear Physics

Supervisor of the master thesis: Dr. Zdeněk Doležal, IPNP

Abstract: The SCT is a silicon strip detector forming a part of the tracking system of the ATLAS experiment at the LHC. The tracking performance of SCT is influenced by several fundamental effects: multiple scattering, Lorentz drift, energy loss variation, noise occupancy, and δ-ray production. In this thesis, the task requested by the SCT detector group has been performed. Clusters containing a δ-ray, which are assigned to a track were studied on data samples, specially prepared for this purpose. A correction to the affected cluster positions was successfully developed. The correction to δ-rays has been implemented into the ATHENA reconstruction framework and its performance was evaluated. A meaningful usage of correction for the detector alignment has been proposed. The ongoing detailed verification of the performance within the event reconstruction is partially beyond the scope of the thesis work.

Keywords: ATLAS, ATHENA, δ-ray, Silicon Strip Detector

Contents

Introduction

The Semi-Conductor Tracker (SCT) is a silicon strip detector forming a part of the Inner Detector of the ATLAS (A Toroidal LHC Apparatus)[1] experiment at the LHC (Large Hadron Collider)[2] used for the track reconstruction. The tracking performance of the SCT is influenced by several fundamental effects: multiple scattering, Lorentz drift, energy loss variation, noise occupancy and δ-ray production. Energy deposits by charged particles in a material lead to the production of low energy secondary electrons, called δ-rays. The position of cluster on track may be distorted by a presence of a δ-ray. In this thesis, δ-rays in SCT clusters assigned to a track were studied on data samples specially prepared for this purpose. The method of δ-ray identification proposed in[3] was further improved to a form extensible to SCT end-caps. A correction to the affected cluster positions was successfully developed. The correction to the position of clusters affected by the δ-ray, which are assigned to a track, has been implemented into the ATHENA reconstruction framework and its performance was evaluated.

Chapter 1 gives an introduction to the ATLAS experiment, describing different sub-detectors, the trigger system and the computing model. Chapter 2 briefly describes the semi-conductor detector principle, the effects of an electromagnetic field on charge carriers and other processes affecting the measurement. Chapter 3 describes the Inner Detector subsystems and refers to the charged particle track reconstruction and the detector alignment. Chapter 4 deals with the analysis of SCT clusters assigned to a track with the position distorted by a δ-ray, thereafter the implementation to the ATHENA framework is described along with the correction performance results.

1. ATLAS Experiment

This chapter describes the ATLAS [1] experiment, which is one of four big experiments at the LHC [2] built at CERN laboratory [1] under the Swiss-French border. The LHC accelerates two counter-rotating proton beams, which collide at four interaction points. The other three experiments are ALICE (A Large Ion Collider Experiment) [4] studying quark-gluon plasma by colliding lead ions, CMS (Compact Muon Solenoid) [5] a second multi-purpose experiment, and LHCb (Large Hadron Collider beauty) [6] studying the properties of b-quark, in particular CP violation.

The ATLAS detector shown in Figure 1.1 is a general-purpose detector split into several cylindrical layers covering almost full angle around the IP (interaction point). With its size of 44 meters in length and 25 meters in diameter, it is the largest collider experiment ever built. It consists of three main sub-detector systems built around the IP. The closest layer to the IP is the Inner Detector (ID) designed to track charged particles. It is briefly described in Section 1.1 and the detailed description can be found in Chapter 3. The Calorimeters, which surround the ID and measure the particle energy, are mentioned in Section 1.2. The outermost part, Muon Spectrometer, which measures muon trajectories and momenta, is briefly described in Section 1.3. The drawing in Figure 1.2 shows the basic idea on how the information from different subsystems is used for particle identification.

In Sections 1.4 and 1.5, the management of the enormous data flow coming from the detector and to the offline analysis is described.

1.1 Inner Detector

The ID [7] shown in Figure 1.3 is used for the reconstruction of momentum of charged particles. the Inner Detector measures the position along the particle trajectory curved in a magnetic field. For this reason the central solenoid encap-

---

[1]The abbreviation is derived from its former French name: Conseil Européenn pour la Recherche Nucléaire, but nowadays the name: European Organisation for Nuclear Research is used.
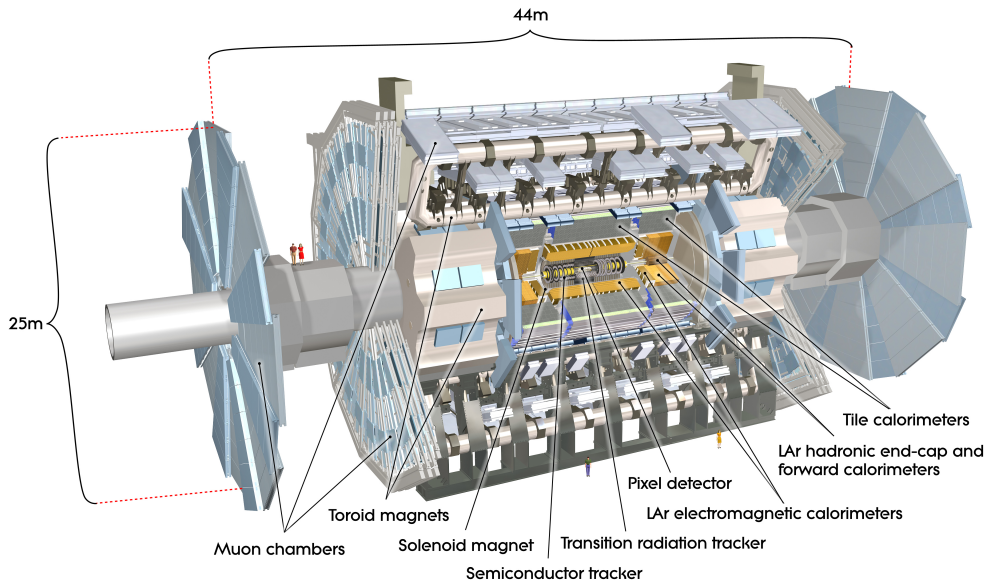
Figure 1.1: The ATLAS is a 44 meters long barrel with a diameter of 25 meters. It weights about 7000 tonnes. Different sub-detectors are indicated. Couple of people are drawn for the size reference.
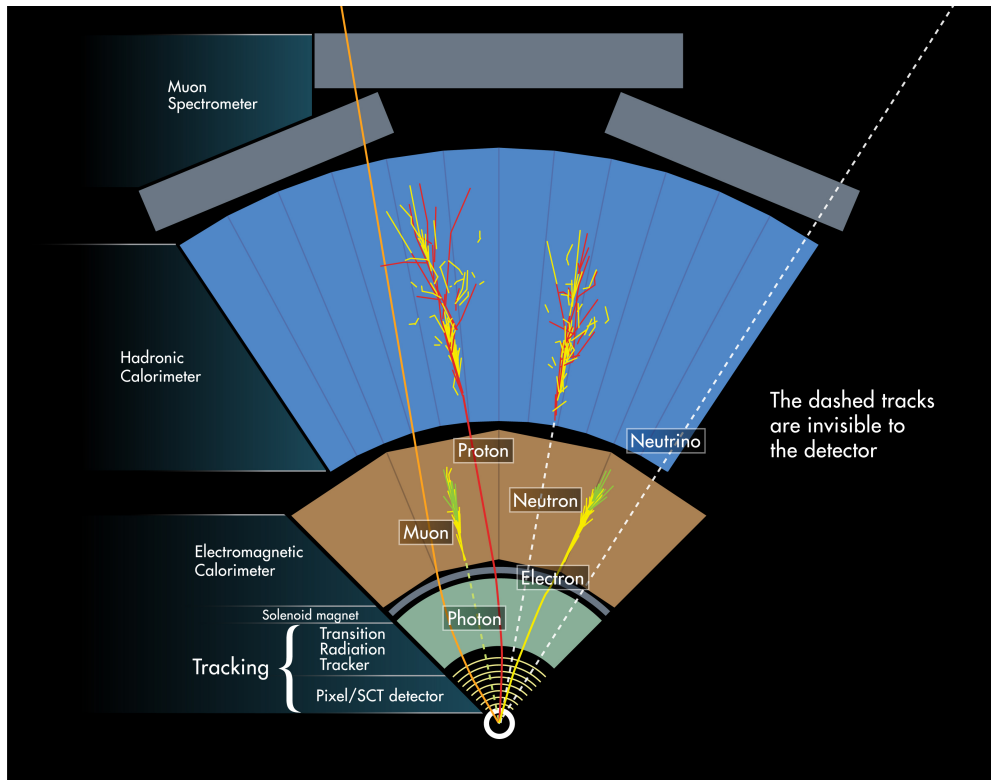

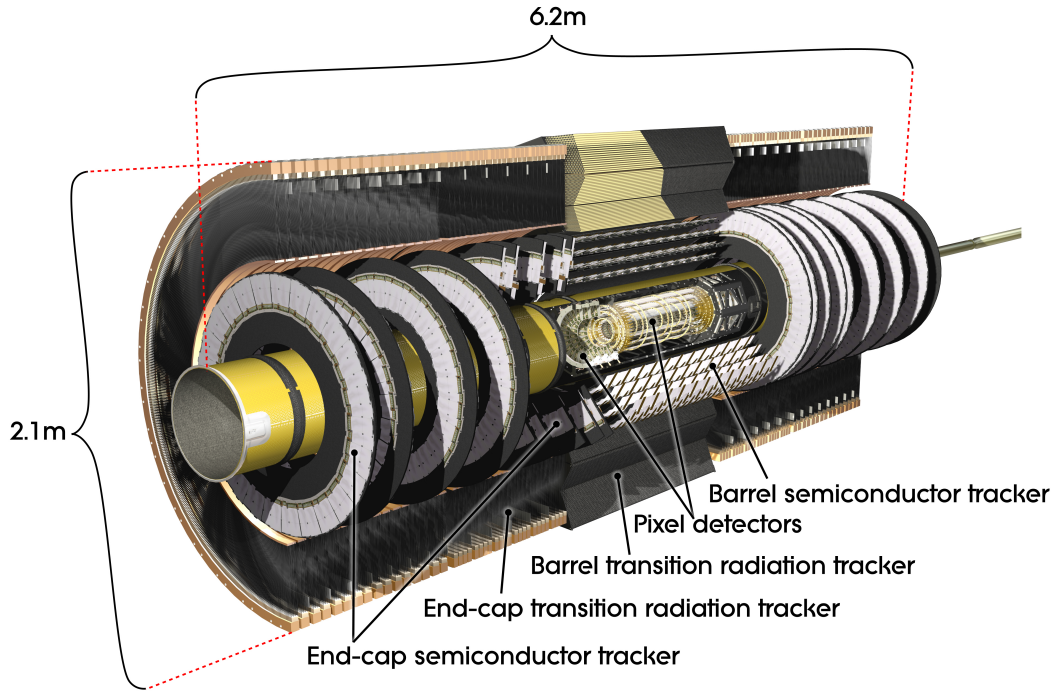Figure 1.2: An image representing how ATLAS detects particles.

6.2m

2.1m

Barrel semiconductor tracker
Pixel detectors
Barrel transition radiation tracker
End-cap transition radiation tracker
End-cap semiconductor tracker

Figure 1.3: An overview of the Inner Detector with different sub-systems indicated.

sulates the ID and provides a magnetic field of 2 T parallel with the beam line throughout the ID volume. A system of different types of detectors is necessary in order to accommodate for the large density of tracks anticipated at the LHC, therefore the ID consists of three subsystems. The silicon Pixel detector, which is the closest sub-detector to the beryllium beam pipe and has the finest granularity, is surrounded by the SCT made of silicon strip detectors. The outermost Transition Radiation Tracker (TRT), consisting of small straws filled by gas. In general, a particle passes through 3 pixel layers and 8 silicon strips (equivalent to 4 space points, since there are 2 layers of wafers in SCT module), and on average there are additional 36 space points per track in the TRT as shown in Figure 3.1. Through the detected positions the curved track is fitted and its primary vertex is calculated. Momentum and vertex resolution requirements are of key importance throughout the experiment. Due to the operating luminosities of the LHC, the ID can withstand only a certain amount of radiation, therefore limiting the detector lifetime (it will be necessary to change it for a new one).

1.2   Calorimeters

The layout of ATLAS calorimeters [8] is shown in Figure 1.4. The task of the calorimeters is to measure the energy of charged and neutral particles. By measuring all these energies, the missing transverse energy (E_T) can be calculated. Missing energy can be caused by neutrinos or possibly by new physics or by bad measurement in calorimeter. To perform a precise energy measurement, the shower created in the calorimeter should be absorbed within the detector volume, therefore calorimeter should be thick enough in terms of radiation length.

The electromagnetic (EM) calorimeter is used for precise energy measurement of electrons, photons, and hardons and for electron and photon identification. A fine segmentation is required, due to the necessity of matching the showers to the measured electron tracks (calorimeter seeded tracks). The EM calorimeter is a liquid-argon detector with lead absorbers, which consists of a barrel part and two end-caps. The barrel as well as the end-caps are further segmented into longitudinal sections with an optimised granularity in η and ϕ for a very good position resolution. The total thickness of the EM calorimeter is more than 22 radiation lengths in the barrel and more than 24 radiation lengths in the end-caps.

The hadronic calorimeter is supposed to provide full-coverage for accurate jet energy and missing (E_T) measurements. A sampling detector with iron absorbers and plastic scintillator plates as the active material is used in the barrel and the extended barrel regions (together forming the Tilecal). At larger pseudo-rapidity the liquid-argon detectors are used. The thickness of hadronic calorimeter is about 10 radiation lengths.

1.3   Muon Spectrometer

The muon spectrometer [9] is the outermost layer of the ATLAS detector, has the largest volume and thereby gives the shape to the whole detector. The layout is based on the usage of large superconducting air-core toroid magnets for the deflection of muon tracks, combined with the use of separate trigger and high precision tracking chambers. Four different chamber technologies are used to fulfil the precision and trigger requirements. The spectrometer is divided into
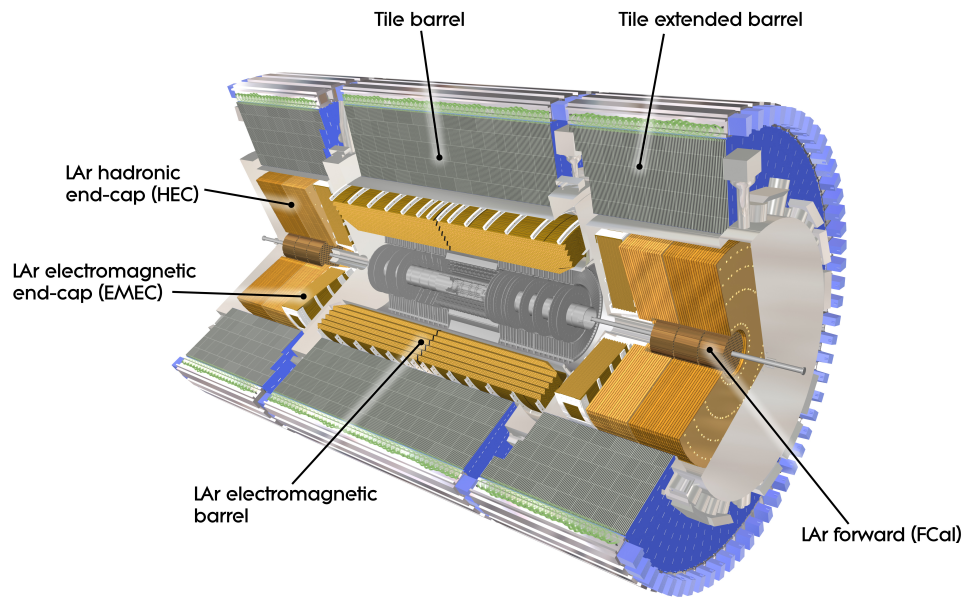
Figure 1.4: A cut-away view of ATLAS Calorimeters with different sub-systems indicated.
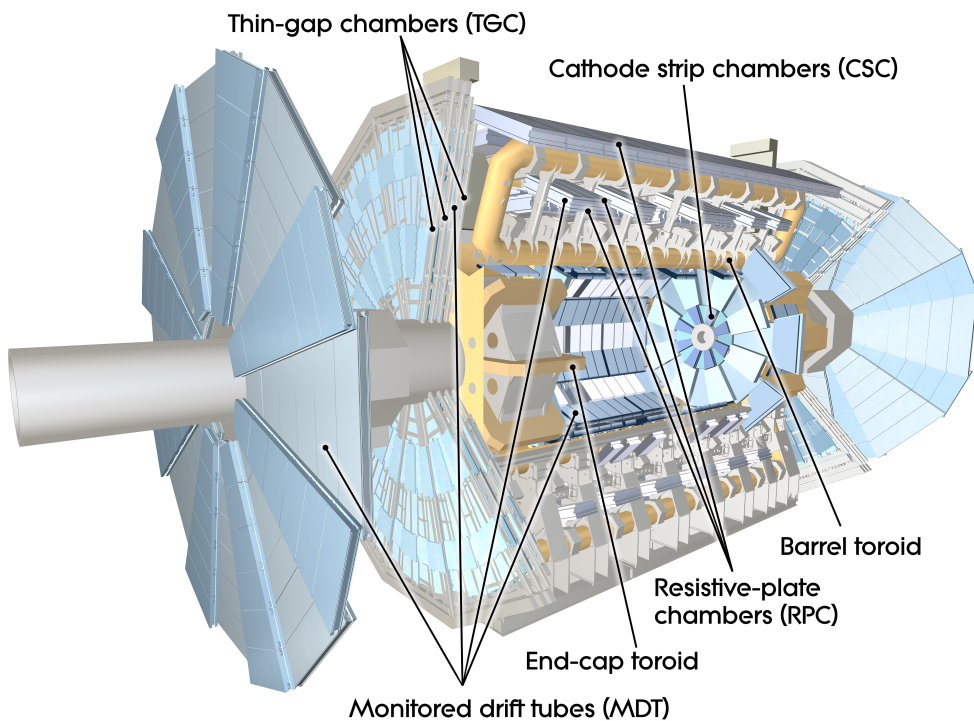

Figure 1.5: A cut-away view of the ATLAS Muon Spectrometer with indication of chambers based on various technologies.

one barrel region and the transition and end-cap regions. In the barrel, chambers are placed in three separate cylindrical concentric layers around the beam axis to measure muon tracks. In transition and end-cap regions, chambers are arranged in four discs. Monitored Drift Tubes and Cathode Strip Chambers provide a precision measurement of muon trajectories in the barrel and end-cap regions. Resistive Plate Chamber in the barrel and Thin Gap Chambers in the end-cap regions together provide the trigger system.

1.4 Trigger

The interaction rate of several hundred millions per second was achieved. Bunches of protons or lead ions are interacting every 50 ns (25 ns respectively) and there are about ninety millions of detector channels, it is impossible to transport and store the information about every interaction that happened. The trigger is designed to pick the interesting physics processes and to reduce the data flow to approximately two hundreds of events recorded per second. Excellent trigger efficiency is required for observing physical processes with very low cross-sections which are the main goals for the ATLAS experiment. The ATLAS trigger works in three levels:

- Level 1 trigger makes the first selection from reduced-granularity information of fast detectors, it combines objects required in coincidence or veto. The first trigger reduces the rate of selected events nominally to 75 kHz.

- Level 2 trigger decides based on the data from regions of interest, surroundings of objects indicated by the level 1 trigger. The level 2 trigger is expected to reduce the rate to 3.5 kHz.

- Event Filter uses offline analysis methods which are simplified to be fast enough for the online analysis. The selected events are stored for the offline analysis. Thereafter output rate of hundreds events per second corresponds to data flow about 400 MB/s.

1.5 Computing Model

The ATLAS computing model [10] deals with the data coming from the Event Filter. Although they are primarily processed at CERN in a Tier-0 facility the system is highly decentralised. The raw data along with the processed data are then distributed to Tier-1 facilities which maintain its storing, further processing and distribution to Tier-2 sites accessible to all collaboration members for analysis. A complex set of tools and distributed services allows the automatic distribution and processing of large amounts of data. A common highly modular framework is used for all levels of data processing, monitoring, online and offline analyses.

1.5.1 Data Types

There are few data types varying in the level of processing and compactness:

- RAW Data is an event based byte-stream format output from the Event Filter, the data has the format of detector output. The files are limited by size of a run (one fill of the LHC) and 2 GB.

- ESD (Event Summary Data) has an object-oriented structure. ESD is an output from primary Tier-0 reconstruction. Its content fulfils requirements of most of the physics analyses, unfortunately not the one aimed by this thesis work. It is stored in POOL ROOT files.

- AOD (Analysis Object Data), further derivate from ESD, already contains physics objects and therefore allows more efficient analysis. It is stored in POOL ROOT files as well as ESD.

- DPD (Derived Physics Data) is the most compact among the basic data types. It is a TTree file format suitable for direct analysis and histogramming, for example using ROOT [11].

1.5.2 ATHENA Framework

The ATLAS software framework ATHENA [10] is derived from the GAUDI framework [12] developed for LHCb experiment. It is based on the blackboard archi-

tectural model [13]. The ATHENA framework consists of C++ classes driven by python configurables and follows the concept by clear separation of data and algorithm classes. The presence of abstract interfaces common for data and algorithms assures an excellent modularity of reconstruction process. Generally, the blackboard system consists of:

- The blackboard, a shared repository. In ATHENA this is the Storegate Service, where all used data objects are stored during the event reconstruction.

- The algorithmic modules, each module reads the blackboard, performs an algorithm and writes again to the blackboard. In ATHENA these modules are called Algorithms (called just once per event) and Tools (can be called many times per event).

- The controller, which controls the flow of the problem-solving activity in the system. In ATHENA this is provided by the Application Manager.

2. Principles of Semiconductor Detectors

The basic building block of a semi-conductor detector is a p-n junction, a diode operated in a reverse bias mode with the depleted area acting as the detection volume. Tracking of charged particles is one of its main applications in high energy physics. When a charged particle passes through a semi-conductor device, it creates electron-hole (eh) pairs. Generally, the hole refers to a vacant position left by the electron. They behave as positively charged particles. A minimum ionising particle (MIP) passing through 285 µm thick silicon creates approximately 25,000 eh pairs. Any charge within the depletion zone will drift towards its borders as a result of the electric field. Under the reverse bias, the current flowing across the depletion region in absence of a real signal is known as the leakage current. It is usually dominated by thermally generated eh pairs which move through the junction as a result of the electric field.

2.1 Charge Carriers in Electromagnetic Field

The charge carriers concentration is as follows [14]:

$$p = n_i e^{\frac{E_i - E_F}{kT}} \tag{2.1}$$

$$n = n_i e^{\frac{E_F - E_i}{kT}}, \tag{2.2}$$

where p (resp. n) is the concentration of positive (resp. negative) charge carriers, n_i is the intrinsic concentration of charge carriers, E_i is the intrinsic energy of the valence band edge, E_F stands for the Fermi's energy, k is the Boltzmann's constant and T is the thermodynamic temperature. The increase of majority carriers is accompanied by a decrease of minority carriers according to the mass-action law:

$$np = n_i^2. \tag{2.3}$$

The velocity $\vec{v}$ of charge carriers in an electric field with intensity $\vec{E}$ is proportional to their mobility μ [15]:

$$\vec{v}_p = \mu_p \vec{E} \tag{2.4}$$

$$\vec{v}_n = -\mu_n \vec{E}. \tag{2.5}$$

In the presence of a magnetic field (with induction $\vec{B}$), the Lorentz force acting on charge carriers is given by the well-known formula:

$$\vec{F} = q\left(\vec{E} + \vec{v} \times \vec{B}\right), \tag{2.6}$$

and thereafter, the movement of charge carriers perpendicular to the magnetic field results in the change of the direction about a Lorentz angle θ:

$$\tan\theta_p = \mu_p^H B \tag{2.7}$$

$$\tan\theta_n = \mu_n^H B, \tag{2.8}$$

where μ^H stands for Halls mobility, which is not exactly the same as mobility. The total conductivity can be written as:

$$\sigma = ne\mu_n + pe\mu_p. \tag{2.9}$$

Obviously, in SCT wafers made of n-type silicon bulk, the hole-based conductivity is negligible with respect to the electron based conductivity.

2.2 Particle Interactions with Silicon

Silicon is a semiconductor with a band gap of 1.1 eV (the electron energy difference between the valence and the conduction band). On average, the energy loss of about 3.63 eV is needed to generate one eh pair. Charged particles ionize the silicon when passing through it, the mean energy loss can be obtained from Bethe-Bloch formula:

$$-\frac{\mathrm{d}E}{\mathrm{d}x} = \frac{4\pi}{m_e c^2} \cdot \frac{nz^2}{\beta^2} \cdot \left(\frac{e^2}{4\pi\varepsilon_0}\right) \cdot \left[\ln\left(\frac{2m_e c^2 \beta^2}{I \cdot (1-\beta^2)}\right) - \beta^2 - \frac{\delta(\beta\gamma)}{2}\right], \tag{2.10}$$

where $\beta = \frac{v}{c}$, v is the velocity of the particle, E the energy of the particle, x the distance travelled by the particle, c the speed of light ze the particle charge, e the electron charge, m_e the rest mass of the electron, n the electron density of the

target, I the mean excitation potential of the target, ϵ_0 the vacuum permitivity and δ describes density effect corrections. With the knowledge of the average energy loss necessary to create eh pair, the integral of mean energy loss can be converted to the number of eh pairs created. Charged particles can knock the electrons in almost perpendicular direction. Such an electron, so called δ-ray, typically has an energy in order of tens or hundreds keV and can create even more eh pairs than the primary particle. This affects the spatial resolution, which is the reason for correction development.

2.3 Processes Affecting the Measurement

Charge carriers accelerated by an electric field drift in a presence of a magnetic field in slightly different direction due to the Lorentz force mentioned above. This effect disturbs the charge collection, Lorentz drift refers to Hall's effect within the detector volume and could be measured.

Silicon is a dense material, therefore particle loses more energy (per unit length). The nature of energy looses is fluctuation having, so called, Landau distribution, it could be a serious change for instance of the energy of the low energy primary particle. Similar to this is the δ-ray, its emission is a product of larger energy loss. The multiple scattering, which is affecting generally the direction of primary particle movement, is similar to these effects. All these effects could be in principle cured by detector thinning.

The last effect to be discussed differs from the others, noise bursts are caused by electrons thermally excited to the conduction band. Thinning will make the noise worse, since for the lower signal, the lower threshold is generally needed.

3. Tracking with the Inner Detector

This chapter refers to the tracking of charged particles with the Inner Detector. At first, the sub-detectors of the ID are described from inside outwards, the Pixel Detector in Section 3.1, the SCT in Section 3.2, and the TRT in Section 3.3. The layout of the ID barrel (resp. end-cap) is shown in Figure 3.1, (resp. Figure 3.2), it indicates the position of various detector elements. Section 3.4 explains the principles of the track reconstruction. The detector alignment is described in Section 3.5.

3.1 Pixel Detector

Located at the closest point to the interaction region, the high precision pixel detector is built as follows: 3 barrel layers segmented in $R\phi$ and z, placed in concentric cylinders around the beam axis, and 3 end-cap discs on each side of the cylinder. The barrels are positioned at radii of approximately $5\,\text{cm}$, $9\,\text{cm}$ and $12\,\text{cm}$ from the beam line. The end-cap discs are placed approximately $5o - 65\text{cm}$ from the IP perpendicular to the beam axis, and are arranged in planes. There are 1744 pixel modules equivalent to 80 million of 8-bit channels. The design of the pixel modules is identical in both the end-cap and barrel layers. Each module measures approximately 63 mm in length and 24 mm in width with the sensor thickness of $250\,\mu\text{m}$. In order to obtain full angle coverage the modules are positioned with a large overlap. With two wafers segmented in both the $R\phi$ and z directions, the readout requires advanced electronics. There are 16 chips per module each with 2880 electronic channels. For every pixel element, read out by its corresponding chip, there is a buffer present in order to store the data and this therefore results in a large chip area.
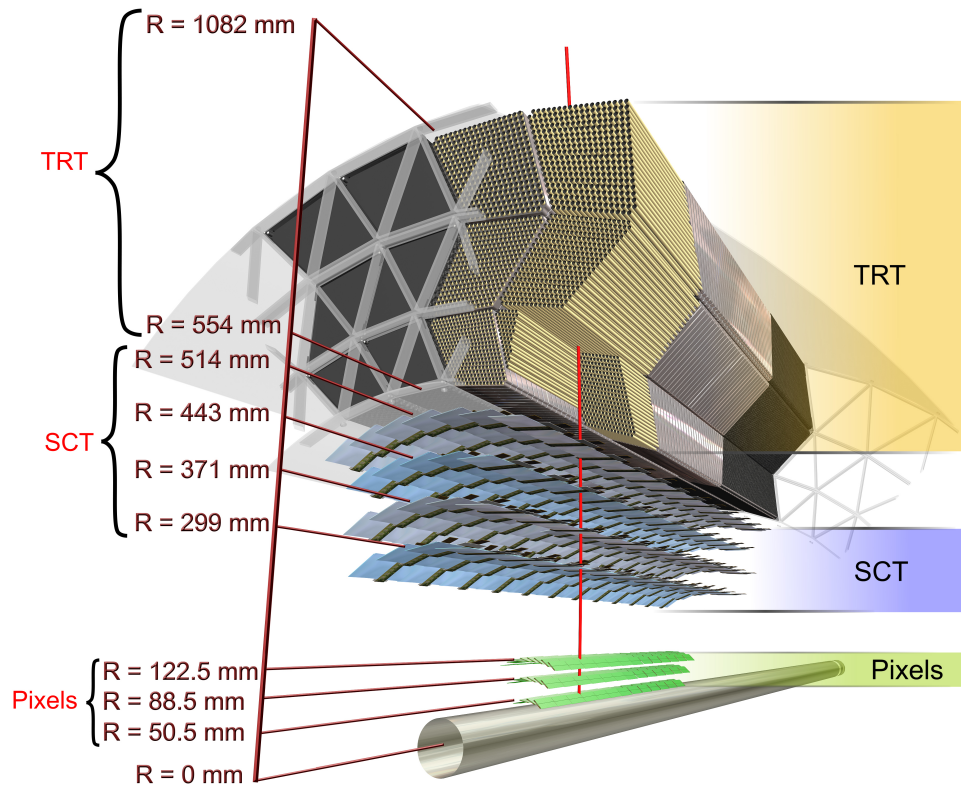
Figure 3.1: A section of the inner detector barrel with the sensors and structural elements traversed by a charged particle. The track crosses successively the beryllium beam pipe, 3 pixel layers, 4 SCT layers and approximately 36 TRT straws.
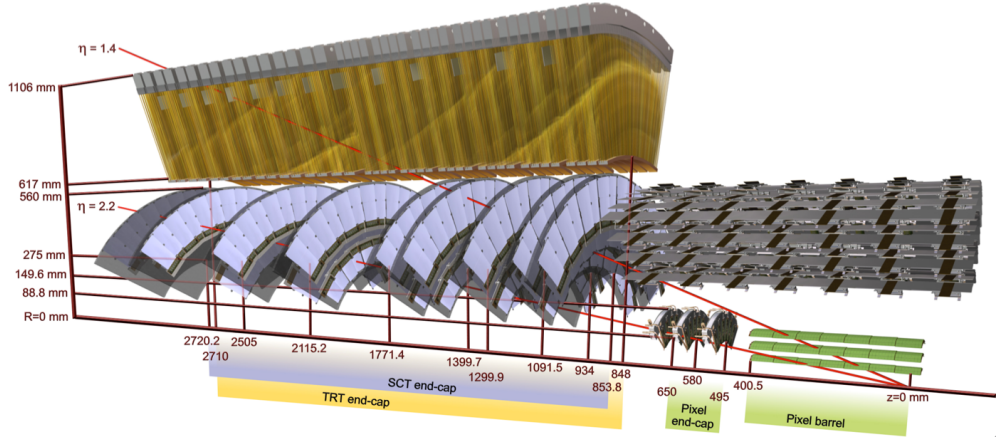
Figure 3.2: A section of the inner detector barrel and end-cap with the sensors and structural elements traversed by two charged particles. Tracks traverse different detector layers in dependence on $|\eta|$. Nominal positions of the detector elements in the end-cap are indicated.

3.2 Semi-Conductor Tracker

The SCT is positioned the second closest to the interaction region, consisting of 4088 modules, with approximately six million readout channels. It comprises of 4 central barrels and two end-caps, each with nine discs. The basic element of the system is a module. Its design provides on average 4 space point measurements for a particle originating from the interaction point up to pseudo-rapidity coverage of 2.5. In total the SCT has an active silicon area of $61\,\mathrm{m}^2$. Silicon micro-strip technology provides fine granularity, which aids significantly the momentum, impact parameter and vertex position measurements. The barrel has only one module type, however four different types are present in the end-cap regions. Each module consists of two layers of silicon wafers $285\,\mu\mathrm{m}$ thick, one runs in parallel or radially and the other rotated to a small stereo angle of 40 mrad. Each module has 768 readout strips per side with a pitch of $80\,\mu\mathrm{m}$. The barrel's four cylinders are placed at different radii from the beam pipe. There are 12 modules associated to each row of the barrel, which are placed in a tile-like manner tilted with respect to the radial direction about 11 degrees for the two inner layers and 11.25 degrees for the two outer layers. For each end-cap, the physics requirements of four space point hits up to $|\eta| = 2.5$, combined with the detector volume constraints, results in a layout consisting of nine discs. The nine discs of each end-cap have between

one and three rings of modules, Outer, Middle or Inner, depending on its position.

The chip electronics is included on the detector itself, consisting of a front-end amplifier, discriminator, and a binary pipeline to store the hits. Binary readout of strips with capacitative charge splitting implies the standard deviation of position measurement in direction perpendicular to strips:

$$\sigma_x = \sqrt{\frac{1}{p} \int_{-p/2}^{p/2} x^2 dx} = \frac{p}{\sqrt{12}}, \tag{3.1}$$

where p is strip pitch.

3.3 Transition Radiation Tracker

The SCT is surrounded by the TRT. It consists of many small diameter (4 mm) straw detectors, enclosing a single gold-plated sense wire. A radiator material layered between the straws allows the identification of electrons by means of detecting transition radiation photons. The TRT provides 36 measurements per track. The barrel contains 52,544 axial straws of 144 cm in length, at radii between 56 cm and 107 cm. The end-caps contain a total of 245760 radial straws at radii between 64 cm and 103 cm. There are 12 inner radius wheels and 8 outer radius wheels to maintain full acceptance. In total there are approximately 300,000 electronic channels, each channel providing a drift time measurement of 130 μm spacial resolution per straw and with two different thresholds. These thresholds distinguish between tracking hits at the lower threshold and transition radiation hits at the upper threshold.

3.4 Track Reconstruction

Tracks are reconstructed in ATLAS software within the ATHENA framework using the reconstruction algorithms described in [16]. To avoid unacceptable increase of CPU time consumption, the simplified detector geometry and material description is used [17], which is in coherence with the ATLAS tracking event data model (EDM) [18, 19].

Pixel clusters are formed from groups of neighbouring pixels with hits. Problematic and noisy channels are rejected at this stage. The knowledge of the posi-

tion of a single pixel cluster is enough to construct a space-point. The neighbouring SCT strips with a hit are grouped into a cluster as well. The one-dimensional clusters from the two sides of a module are combined into the three-dimensional space-points using the knowledge of the stereo angle and the radial (longitudinal) positions of the barrel (end-cap) modules. The three-dimensional space-points in the pixel detector and the SCT, together with drift circles in the TRT are filled as an input to the pattern recognition algorithms.

Track seeds are formed from sets of three space-points in the silicon detectors, originating in a different layer. Track candidates are formed by seeds and clusters found within the road defined by the seed. Obviously, each cluster can be attached to several track candidates. Then the poor track candidates are rejected by ambiguity-resolving algorithm to have each cluster assigned to a maximum of one track. A track fit is performed to the clusters associated to each track. Tracks are then matched to drift circles in TRT and a combined fit throughout whole inner detector is performed[20]. The tracks are required to have at least seven hits in the SCT and at least two hits in the pixel detector (for the analysis purposes tracks were required to have at least eight SCT hits, three Pixel hits and at least ten TRT hits, in this way to be better defined).

3.5   Detector Alignment

The alignment of the inner detector (both internal and with respect to the other detectors) is critical to obtain the optimal tracking performance. The design requirement is that the resolution of track parameters shouldn't be degraded by more than 20% with respect to the intrinsic resolution. The method to determine the ID alignment uses a χ^2 technique that minimises the residuals to fitted tracks[21]. Alignment is performed sequentially at different levels of detector granularity starting with the largest structures followed by alignment of individual layers and finally the positions of individual modules are optimised. The number of degrees of freedom at the different levels increases from few tens at the first level to few tens of thousands at the module level.

4. Correction to Delta Rays

This chapter describes the development of the correction to the position of clusters on a track containing a δ-ray in the SCT sub-detector. The method for identifying silicon hit clusters that are larger than expected from the reconstructed track was proposed in [3], where the rate and range of δ-ray production in silicon layers of the Inner detector barrel were studied. This method was further improved in terms of the δ-ray identification, especially its extensibility to the end-caps. For the δ-ray candidate SCT clusters assigned to a track, the correction was developed, implemented and verified. Section 4.1 defines δ-rays, and how they influence the detector readout, as well as it defines a set of parameters for studying them. In Section 4.2, the production of appropriate data for the analysis is explained, since the previously used ntuples were no longer supported. Section 4.3 refers to the debugging and analysis performance boost. Section 4.4 refers to the analysis procedures and its results are presented in Section 4.6.

4.1 Delta Rays in Clusters

Energy depositions by charged particles in a silicon leads to the production of low energy secondary electrons, called δ-rays, as mentioned in Section 2.2. They may produce even more electron-hole pairs than the primary particle and therefore broaden the cluster to neighbouring strips, which were not traversed by the primary particle, and which biases the position measurement. The charge collected from a primary particle can extend just over a certain number of strips, and the observed clusters larger than this arise primarily from the δ-ray production. The effect of a δ-ray to the SCT cluster is illustrated in Figure 4.1. Neglecting the effects of charge diffusion and multiple Coulomb scattering, the expected width W_e of a cluster from a track with incident angle α is given by

$$W_e = t \cdot (\tan \alpha - \tan \theta_L), \tag{4.1}$$

where t is the sensor thickness and θ_L is the Lorentz drift angle. This is the physical extent of the charge deposition reaching the surface of the sensor, and so far independent of a sensor segmentation. The expected width is a quantity that

is precisely determined, and clusters wider than permitted by incident angle are candidates for being caused by δ-rays. The production of a single δ-ray adds strips to one side of the cluster, leading to a shift in the cluster centroid, thereafter the track residuals are shifted of approximately $(W_o \cdot p - W_e)/2$, where W_o is observed width of cluster. Another possible cause of a cluster broadening is the merging of two randomly overlapping clusters from different tracks. The information about the presence of a merged cluster is to be kept from the reconstruction procedure to allow evaluation of its impact on analysis and also the possible exclusion. The rate of δ-ray production is expected to change with the track $\beta\gamma$ according to the Bethe-Bloch Equation 2.10. The aim of this work is to correct cluster positions distorted by a δ-ray once tracks have been found and in this way to improve the track parameters once refit.

4.2 Data Production

The first intended step was to reproduce and extend the previous analysis [3]. Unfortunately, the previously used Track Validation ntuples are no longer supported. Several centrally produced dataset types were investigated for the information needed to perform the analysis. Global track parameters and track summary were needed to perform track quality cuts. Local track parameters with respect to module wafer, the Lorentz angle measurement and the cluster on track properties are the most important input data. No datasets containing all the necessary parameters were found. The least amount of missing parameters were found in old non-supported Track validation ntuples (just the summary of merged clusters was missing).

To add branches about shared clusters, it was found necessary to run the event reconstruction with RAW data as an input since even ESDs are not containing this information. For the data production and latter for the analysis ATHENA version 17.2.4.4 was used. A tool, where to add a number of shared hits on track was identified:

`TrkValidation/TrkValTools/src/MeasurementVectorNtupleTool.cxx`

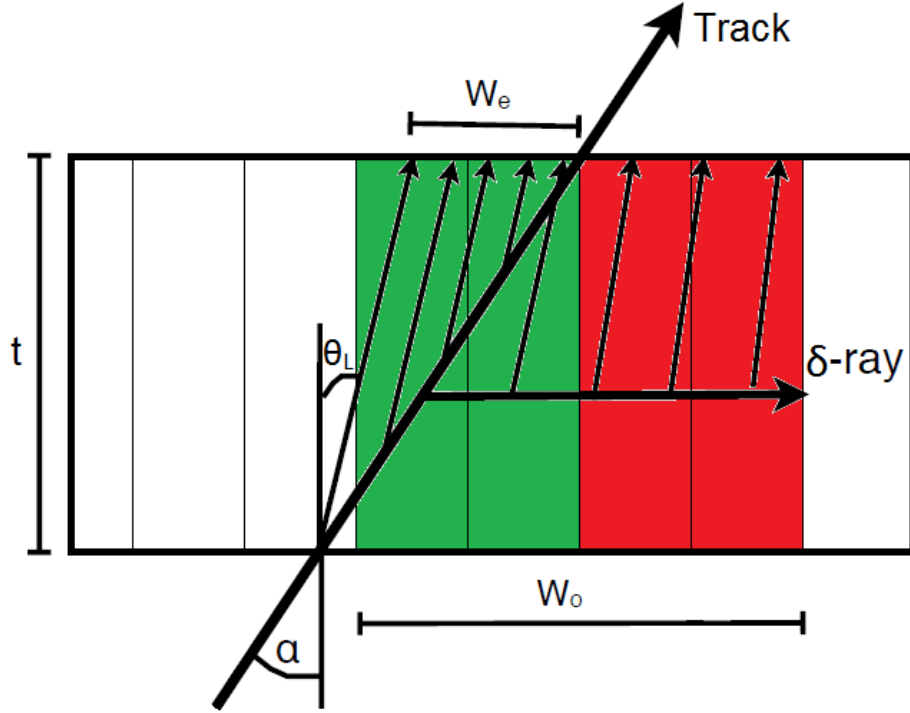Job option file to be steered and run for this purpose is located:

Figure 4.1: The schematic view of SCT detector sensor section in the plane perpendicular to the direction of strips. Here a fitted track of the particle traversing through the sensor is "emitting" a δ-ray. The strips fired by a primary particle (holding the information to be reconstructed) are shown in green, while strips fired by the δ-ray (creating a position bias to be corrected) are shown in red. The quantities noted are: sensor thickness $t = 285$ μm, the observed width of cluster W_o, the expected width without the δ-ray W_e, track incident angle α, and the Lorentz drift angle θ_L.

```
InDetExample/InDetRecExample/share/jobOptions_Standalone.py
```
The Grid Computing Network was used for the data reconstruction, since the CPU time needed to reconstruct one event is in the order of few minutes.

4.3   Skimming, Thinning and Slimming

The Track Validation ntuples consist of track and hit trees, linked to the main event based tree. For the purpose of an efficient analysis, the file structure was impractical and containing a lot of unused data, at the same time there was a need to reduce the processing time. At first, the size of the ntuples was about 1.5

times larger than size of the original RAW data. In principle, the reconstruction and ntuple creation was steered in a way that most of the data originally present was not even calculated, the list of major changes is as follows:

- `InDetExample/InDetRecExample/share/InDetRecNtupleCreation.py`
  -Removing of Track and Hit PositionNtupleHelper (Track and Hit Position branches from TrkValidation ntuple)

- `TrkValidation/TrkValTools/src/`
  `ResidualValidationNtupleHelper.cxx`
  -Branches containing residual and pull information about hits from subdetectors other than SCT removed

- `TrkValidation/TrkValTools/src/TrackInformationNtupleTool.cxx`
  -Unused branches containing info about tracks removed

- `TrkValidation/TrkValTools/src/MeasurementVectorNtupleTool.cxx`
  -Removing Holemaker and ResCalculator tools
  -Removing helper tools for outer parts of ATLAS detector
  -Removing hitIndices (linking branches to specific hits on track)

- `InDetValidation/InDetTrackValidation/src/`
  `SiResidualValidationNtupleHelper.cxx`
  -Steering of SctTrk ntuple part content

Once the thinned and slimmed ntuples were produced, track quality cuts shown in Table 4.1 were applied. Then, the information to identify the event (RunNumber, EventNumber and the number of reconstructed tracks) was added to the cleaned track based tree already containing relevant SCT cluster on track properties. The size of the ntuple was decreased to about $0.04\,\%$ of the input RAW data size.

4.4   Data Analysis

The analysis is carried out with data collected by the ATLAS detector in 2012. The most relevant data is from the Minimum Bias stream of rather short ($56\,\mathrm{nb}^{-1}$) low multiplicity Run Number 201351.

at least 3 pixel hits
at least 8 SCT hits
at least 10 TRT hits
$p > 1\,\text{GeV}$
$|z_0| < 75\,\text{mm}$
$|d_0| < 5\,\text{mm}$

Table 4.1: The track quality cuts

As a first step, the main part of ROOT based analysis from [3] was reproduced for the SCT barrel to check the behaviour and eventually to validate the data reconstruction. Thereafter, the necessary quantities to be analysed were calculated within the ATHENA framework instead of ROOT, specifically in `SiResidualValidationNtupleHelper.cxx` mentioned above.

By excluding all tracks with shared clusters, it is expected to virtually eliminate merged clusters from the δ-ray sample. The exception would be merged clusters where one of the tracks involved is not reconstructed. After all quality cuts applied, there are only about $2\,\%$ of tracks with a δ-ray candidate containing a shared cluster. So even before the shared cluster rejection, the contribution of shared clusters is negligible.

The number of single δ-rays is estimated by fitting the residual distributions to the sum of two Gaussian functions: one for the signal peak with a mean away from zero and one for the background with a mean at zero. Only unbiased residuals were used, meaning that in the calculation of the track residual, the specific hit is excluded to prevent biasing of the track by the analysed cluster.

4.4.1 Candidate Finding Algorithm

Using the incidence angle and the Lorentz drift angle, the expected width W_e of the cluster is calculated according to Equation 4.1. The important difference to the previous study [3] is the incidence angle not taken as a projection to $\text{R}\phi$ plane, but as an angle around the axis parallel to the strip fired. This allows the extension to the end-caps, where the concept of expected width is preserved in this way. In the barrel, the two different incident angles are well correlated as the
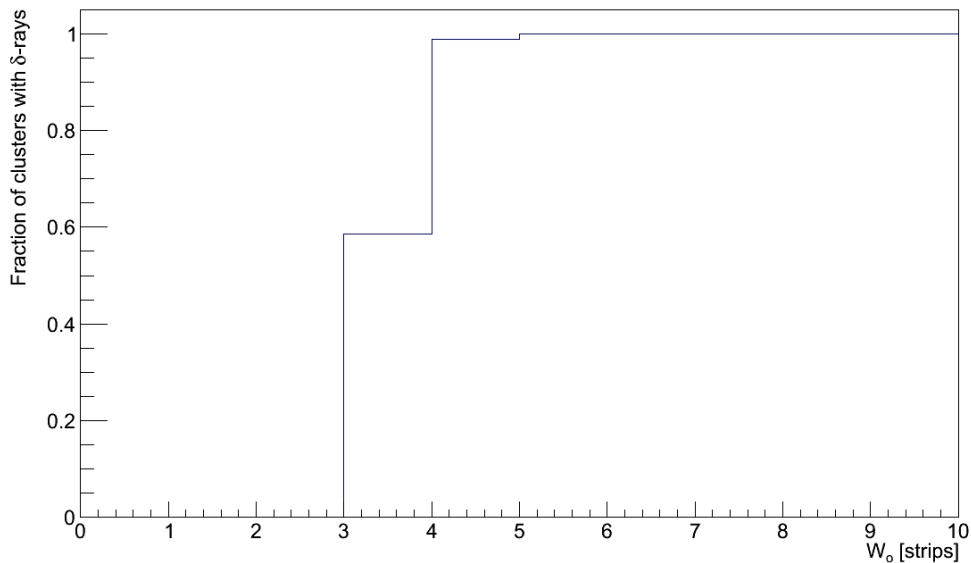
Figure 4.2: A fraction of clusters on a track, which are distorted by a δ-ray, as a function of the observed width of cluster. Note that for cluster size equal or higher than four stripes, there are almost no clusters without a δ-ray.

disruption coming from the stereo angle (40 mrad) is negligible. The tilt of the detector with respect to the radial direction (11 degrees for the two inner layers, 11.25 degrees for the two outer layers) does not compensate for the Lorentz drift angle (currently around 4 degrees), and therefore tracks curved in one direction will have, on average, smaller absolute expected width than those curved in the opposite direction. The transverse momentum of particle hitting the barrel gives a geometrical restriction to incident angle via formula:

$$p_T \, [\text{GeV}] = 0.3 B \cdot R \, [\text{T} \cdot \text{m}] \, . \tag{4.2}$$

Neglecting the diffusion and scattering processes, hits for which the absolute value of W_e is less than $(W_o$ - 2$)$ times strip pitch are identified as a candidate for the δ-ray. In Figure 4.2 the fraction of clusters with a δ-ray in dependence on the observed width of the cluster is shown. There are almost no big clusters without δ-ray (this quantity depends on the particle momentum). In Figure 4.3 the fraction of clusters with a δ-ray in dependence on the particle momentum. The behaviour is almost constant, and therefore doesn't correspond to Bethe-Bloch formula, probably due to small statistics and no cut to particle type.
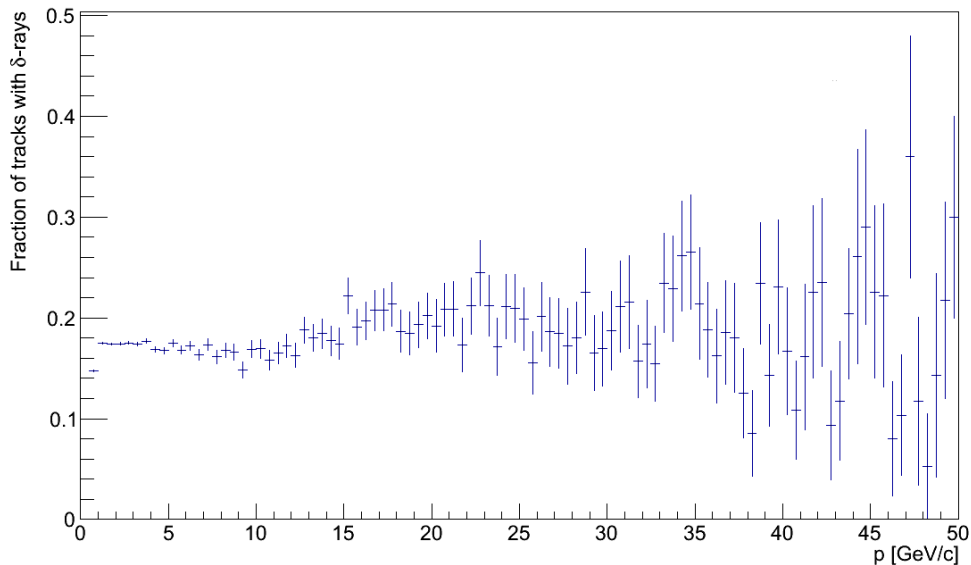
25

Figure 4.3: A fraction of clusters on a track, which are distorted by a δ-ray, as a function of the track momentum.

4.4.2 Residual Distribution

Only single δ-ray clusters should be separated, excluding multiple δ-rays and other possible backgrounds. This background is expected to contain multiple δ-ray clusters, scattered primary particles, electronic charge sharing effects etc. The production of a single δ-ray adds strips to one side of the cluster, leading to a shift in the cluster centroid, thereafter the track residuals are shifted of approximately $(W_o - W_e)/2$. A negative and a positive peak are corresponding to δ-rays travelling to left or right (merged different peaks from the barrel and end-caps). Fitting the residual magnitude rather than signed residuals assumes the signal peak shifts are symmetric about zero, which was empirically verified as well as the symmetry in the sign of W_e. Therefore, the plots can be folded onto the positive W_e and residual quadrant. This analysis exploits a characteristic shift of the track residual distributions caused by δ-rays or merged clusters using the inconsistency between the observed cluster size and the expected size from the reconstructed track. The mean value of "signal" residual Gaussian (shown in Figure 4.4, where the sum of two Gaussians is fitted to the sample data) is used as a correcting shift to the cluster on track position perpendicular to the strip direction and at the same time towards the track position. Figure 4.5 shows a
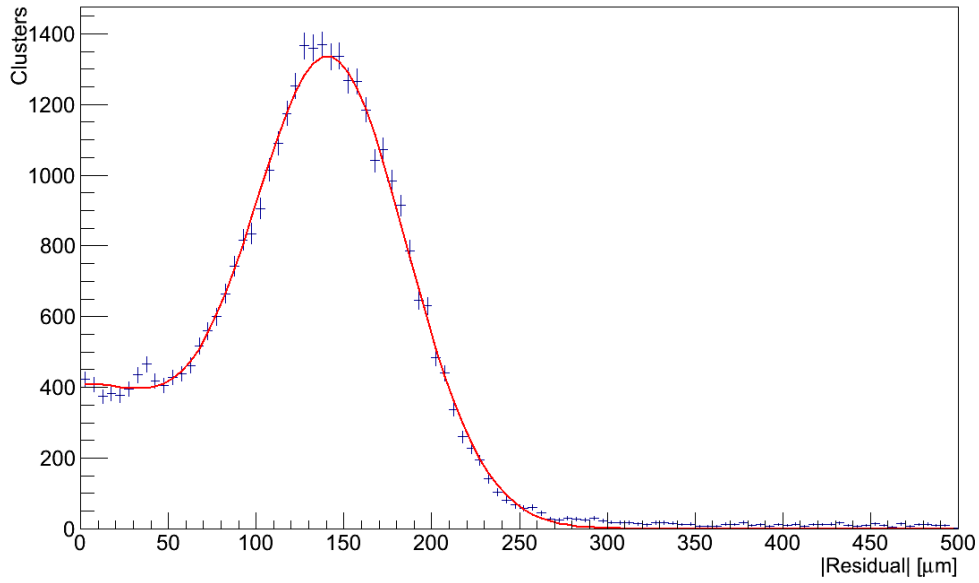
Figure 4.4: A residual distrubution of a δ-ray candidate data sample with the observed width of 5 strips, and the smallest bin of absolute value of expected width. The fit with two Gaussians (one centred at zero, the other centred at mean value of further correction) is performed.
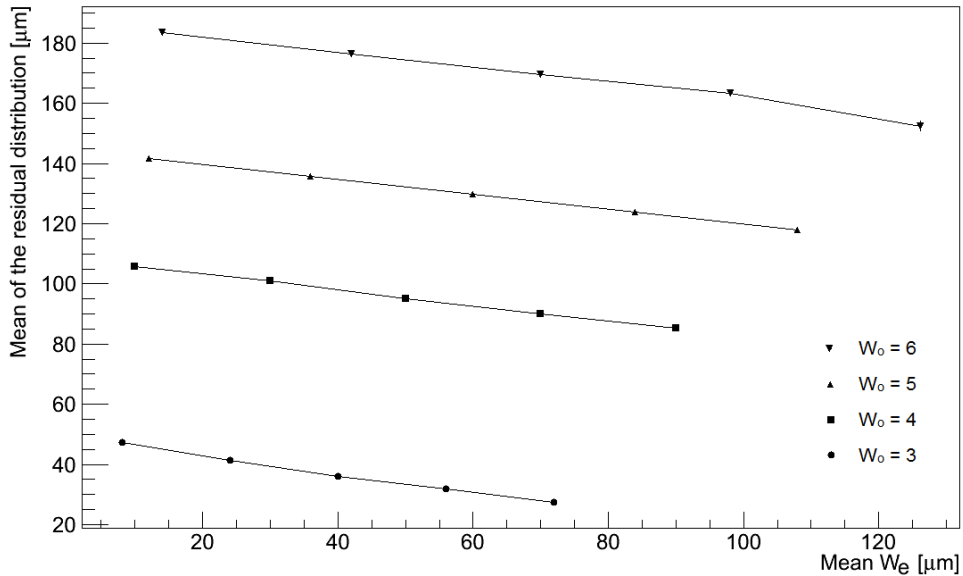

Figure 4.5: A combined plot shows fitted means of residual signal Gaussian distributions of δ-ray candidate data samples (similar to the one shown in Figure 4.4) with various widths (observed and expected).

27

combined plot of mean value of "signal" residual Gaussians for different cluster widths (either observed and expected). These results are in agreement with [3]. The dependence of the residual distribution of clusters disturbed by δ-rays on the other parameters (for instance the path length, η) was studied. No useful dependency was found for the correction of a cluster position.

4.5   Implementation of the Correction

In this section, the implementation procedure is described. Before the cluster position can be corrected, tracks have to be fitted and ambiguities rejected. The place to implement the correction is a tool which creates SCT clusters from `Trk::PrepRawData` and has track parameters `Trk::TrackParameters` to identify the δ-ray candidates and calculate the size of correction. Such a tool was identified in

`InDetRecTools/SiClusterOnTrackTool/src/SCT_ClusterOnTrackTool.cxx`.

The correction was implemented with a decision to which direction to move the local cluster position based on the comparison of the local cluster position and the local position of the track intersection with the sensor wafer.

The correction could be steered (with no need for recompilation) by a boolean property `SCTDeltaRayCorrection` of `SCT_ClusterOnTrackTool` in

`InDetExample/InDetRecExample/share/InDetRecLoadTools.py`.

The correction (the size of the cluster position shift) is implemented in a linear form coming from fits of data shown in Figure 4.5. The linear form works smoother than a usage of an artificial binning and a lookup table:

$$x\,[\mu\mathrm{m}] = \left(40 \cdot W_o - 50 - \frac{|W_e|}{3.8}\right)[\mu\mathrm{m]\,,} \tag{4.3}$$

for a cluster width of more than three strips(40 refers to a half of strip pitch), and:

$$x\,[\mu\mathrm{m}] = \left(50 - \frac{|W_e|}{3.8}\right)[\mu\mathrm{m}]\,, \tag{4.4}$$

for an affected cluster consisting of three hit strips. The error of a cluster position measurement is, while correcting the position, kept unchanged. No effect on tracks was observed, when reducing appropriately the error, because there is

usually just one cluster on the track affected by the δ-ray and this is moved close to the intersection of the track and the detector wafer. No effect was observed even in end-caps, where neighbouring SCT strips are not parallel, and therefore the error ellipse was rotated.

4.6   Results

In this section the most important results are discussed. The procedure to correct the position of the SCT cluster assigned to a track, which is distorted by a δ-ray, starts with its identification. Here, the aim was to develop an algorithm, which identify all the cluster on a track with a δ-ray and do not identify any cluster on a track without a δ-ray. The identification is improved with respect to [3], the algorithm finds more clusters with δ-rays with negligible increase of misidentification. The typical background is around 10 % of clusters, need to mention that in dependence on the expected and observed width, the background distribution is not uniform. No other parametrization appeared to be more sensitive in terms of width of the "signal" residual Gaussian. Using the track incident angle defined as perpendicular to the detector plane and at the same time to the strip direction instead of projection to $R\phi$ plane allowed to extend the correction in the SCT end-caps.

The measurement of the correction size follows the same principles as the identification algorithm (when it is easy to find a "signal" residual Gaussian, it is also easy and precise to calculate its mean value). Statistical error (coming from the correction of a cluster without a δ-ray) can be estimated to 10 % as well. The precision of the mean residual Gaussian value is much better due to the higher statistics. It may be around one μm, few μm at most.

The performance of the correction is evaluated by a comparison of the histograms (showing the number of δ-ray candidate clusters in dependence on the absolute value of residual and the absolute value of W_e with W_o fixed) before and after the correction. Such a histogram before (resp. after) the correction is shown for the cluster size of four strips in Figure 4.6, (resp. 4.7). These histograms for various cluster sizes are shown in the attachment, Figures 1-6.
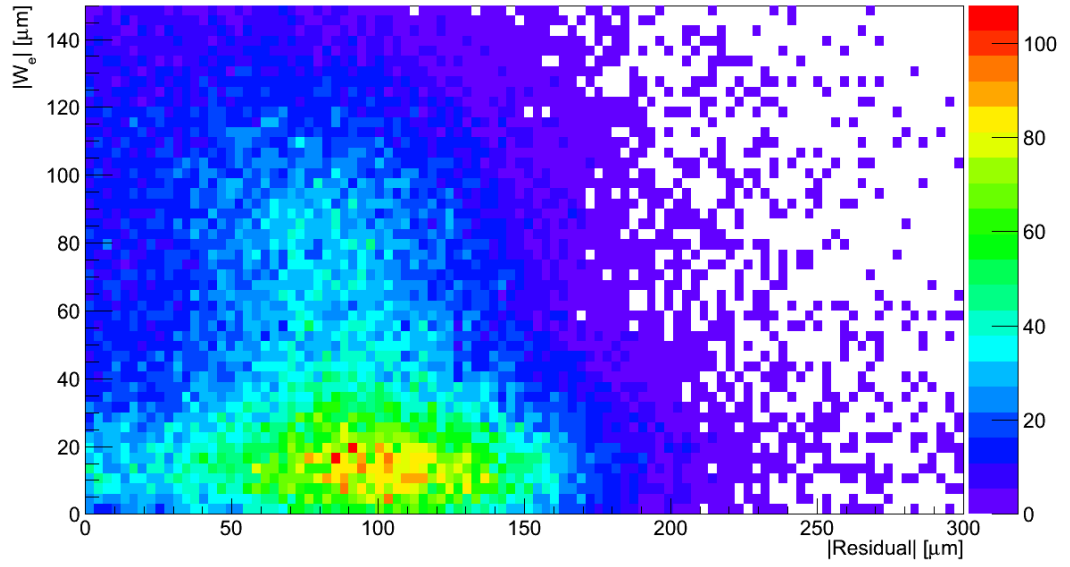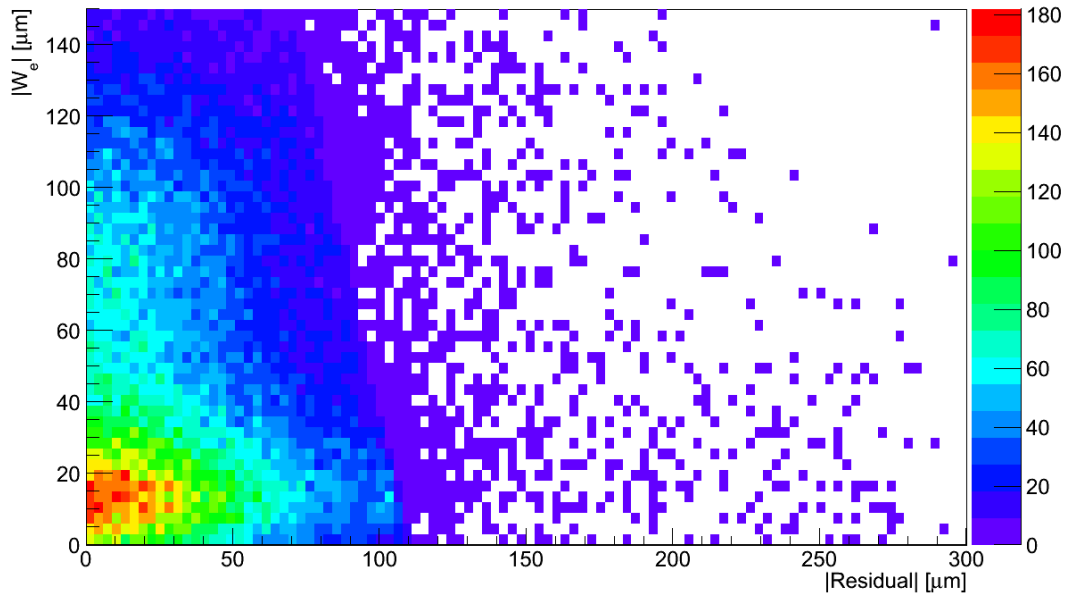
Figure 4.6: The plot of the absolute value of residuals versus the absolute value of the expected width of the cluster ($W_o = 4$) on a track disturbed by the δ-ray before the correction. The "signal" Gaussian is clearly visible and centred away from zero in residuals.
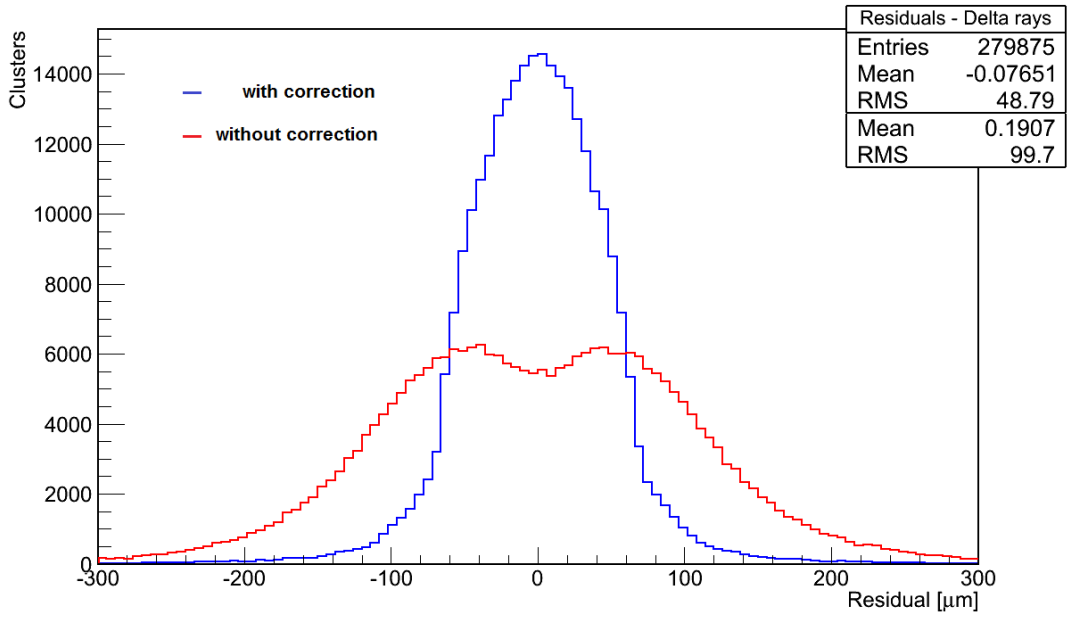

Figure 4.7: The plot of the absolute value of residuals versus the absolute value of the expected width of the cluster ($W_o = 4$) on a track disturbed by a δ-ray after the correction. The "signal" Gaussian is clearly visible and centred at zero in residuals.

Figure 4.8: The sample of the residual distribution of identified δ-ray candidate clusters on a track before correction (resp. after correction) shown in red (resp. in blue). The width of distribution is squeezed by factor of 2.
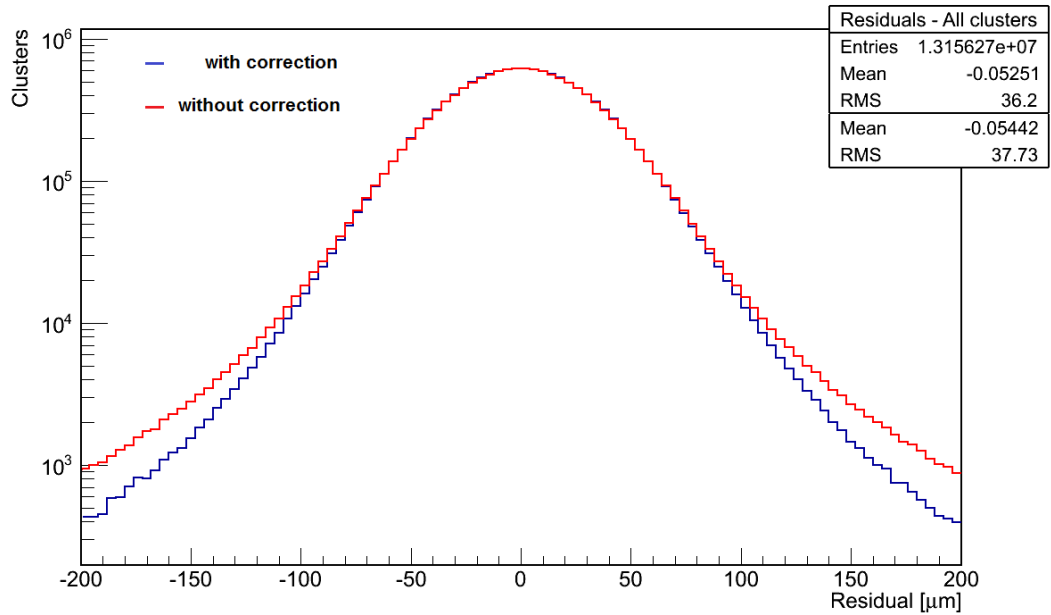

Figure 4.9: The residual distribution of the whole sample before correction (resp. after correction) shown in red (resp. in blue). The width of distribution is squeezed by about 4 %. The logarithmic scale is here to show the difference in tails.
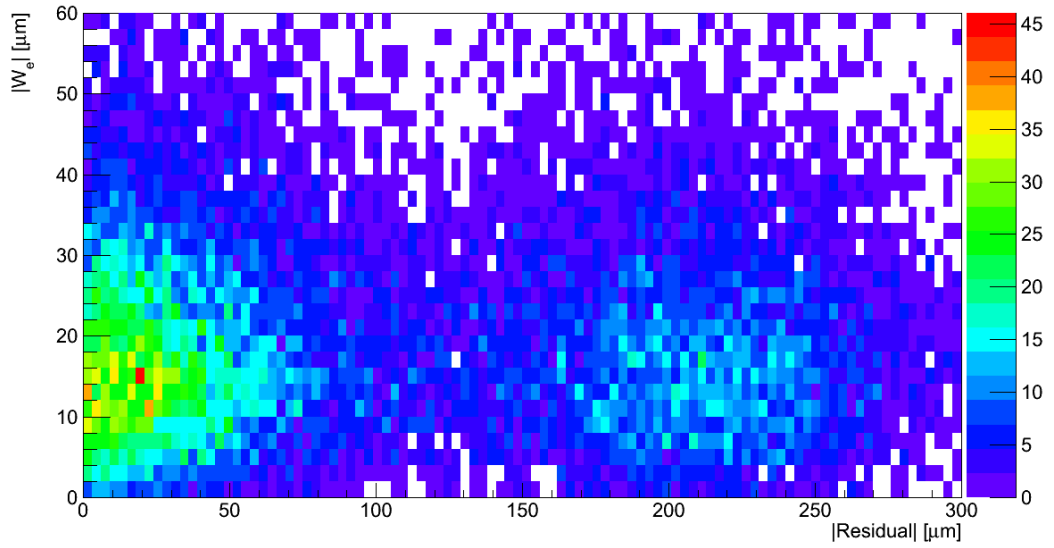
Figure 4.10: The plot of the absolute value of residuals versus the absolute value of the expected width of the cluster on track disturbed by the δ-ray. Note the bump with the absolute value of residuals centred around 200 µm, while for this sample the correction was about 100 µm.

In general, the correction reduces the width of the residual distribution of δ-ray candidate cluster downto RMS $= 49$ µm. This corresponds to a relative decrease of residual width about 4 % for the whole dataset. Figure 4.8 presents the residual distribution of a corrected data with a δ-ray in a cluster (in blue) compared to the data before the correction (in red). In Figure 4.9 the whole data sample is shown.

Unfortunately, a discrepancy in the direction of the correction appeared in about 30 % of clusters on tracks in SCT end-caps, as shown in Figure 4.10. It is a subject to further study whether this is due to a wrong geometry description of the local axis definition. Several additional checks have been performed and potential source (for instance, $\eta\,\phi$ dependency, specific disc/layer, error matrix rotation or swaped sign of the local position) excluded.

Conclusions

This thesis work was performed at CERN laboratory within the ATLAS experiment built around the one of the beam intersection points at the LHC. The aim was to improve the tracking performance by correcting the position of SCT clusters on a track, which may be distorted by secondary electrons (called δ-rays) knocked on by primary particles, while traversing the detector bulk.

SCT detector group needed to study and correct the position of SCT clusters affected by δ-rays. After an extensive work on the data production, the possibility to correct cluster on track positions distorted by δ-rays was studied. The method of δ-ray identification proposed in [3] was further improved to a form extensible to SCT end-caps. The correction for the position (perpendicular to the strip direction) of cluster containing a δ-ray was developed, and has been implemented into the ATHENA framework and verified for most of the cases [1].

A δ-ray is present in about $17\,\%$ of tracks, usually with one candidate cluster per track, what makes the direct effect on a momentum measurement precision negligible. The correction decreases the width of the cluster position residual distribution by a factor of 2 for the candidate subset as shown in Figure 4.8, which corresponds to $4\,\%$ residual decrease for the whole dataset as shown in Figure 4.9. Rather conservative error strategy of correction has been applied, due to the self-biased nature of the correction method. The correction visibly improves the position measurement precision and therefore can be used to perform a better detector alignment. When used for the alignment, the improvement may be seen, nevertheless the effect of the correction to clusters on track will be probably small.

---

[1]The study of the artefact found in the end-caps mentioned in Section 4.6 and shown in Figure 4.10 is still ongoing.

References

[1] The ATLAS collaboration, The ATLAS Experiment at the CERN Large Hadron Collider, JINST 3 (2008) no. 08, S08003.

[2] O. Brüning, et al., *LHC Design Report*, CERN, Geneva, 2004

[3] T. Mueller and M. Garcia-Sciveres, *Measurement of delta rays in ATLAS silicon*, ATL-COM-PHYS-2011-1024, 2011.

[4] The ALICE Collaboration, The ALICE experiment at the CERN LHC, JINST 3 (2008) no. 08, S08002.

[5] The CMS Collaboration, The CMS experiment at the CERN LHC, JINST 3 (2008) no. 08, S08004.

[6] The LHCb Collaboration, The LHCb Detector at the LHC, JINST 3 (2008) no. 08, S08005.

[7] ATLAS Collaboration, *ATLAS Inner Detector: Technical Design Report, 1*, CERN, Geneva, 1997.

[8] ATLAS Collaboration, *ATLAS Calorimeter Performance: Technical Design Report*, CERN, Geneva, 1996.

[9] ATLAS Collaboration, *ATLAS Muon Spectrometer: Technical Design Report*, CERN, Geneva, 1997.

[10] ATLAS Collaboration, *ATLAS Computing Technical Design Report*, 2005.

[11] R. Brun and F. Rademakers, *ROOT: An Object-Oriented Data Analysis Framework*, Linux Journal **51**, 1988.

[12] G. Barrand et al., *GAUDI - A software architecture and framework for building HEP data processing applications*, Comp. Phys. Comm. **140** (2001) 45.

[13] R. S. Engelmore and A. Morgan, *Blackboard Systems*, Addison-Wesley Publishing Company, New York, 1988.

[14] Lutz G., *Semiconductor Radiation Detectors*, Springer, Berlin, 1999.

[15] Doležal Z., *Polovodičové detektory v jaderné a subjaderné fyzice*, lecture notes, `http://www-ucjf.troja.mff.cuni.cz/ dolezal/teach/semicon`, 2007.

[16] T. Cornelissen et al., *Concepts, Design and Implementation of the ATLAS New Tracking (NEWT)*, ATL-SOFT-PUB-2007-007, 2007.

[17] A. Salzburger et al., *The ATLAS Tracking Geometry Description*, ATL-SOFT-PUB-2007-004, 2007.

[18] P.F. Akesson et al., *ATLAS Tracking Event Data Model*, ATLAS-COM-SOFT-2006-005, 2006.

[19] T. Cornelissen et al., *Updates of the ATLAS Tracking Event Data Model (Release 13)*, ATLAS-COM-SOFT-2007-008, 2007.

[20] T. Cornelissen et al., *The global χ^2 track fitter in ATLAS*, J. Phys. Conf. Ser. **119** (2008) 032013.

[21] S.-C. Hsu, *Alignment of the ATLAS Inner Detector Tracking System*, Nucl. Phys. Proc. Suppl. **215** 1325 (2011) 92.

List of Abbreviations

ALICE	-	A Large Ion Collider Experiment
AOD	-	Analysis Object Data
ATLAS	-	A Toroidal LHC Apparatus
CERN	-	Conseil Européenn pour la Recherche Nucléaire
CMS	-	Compact Muon Solenoid
DPD	-	Derived Physics Data
EDM	-	event data model
eh	-	electron-hole (pair)
EM	-	electromagnetic
ESD	-	Event Summary Data
ID	-	Inner Detector
IP	-	Interaction Point
LHC	-	Large Hadron Collider
LHCb	-	Large Hadron Collider beauty
MIP	-	minimum ionising particle
Missing E_T	-	missing energy in the transverse plane
SCT	-	Semi-Conductor Tracker
TRT	-	Transition Radiation Tracker

Attachments

Attached Figures 1- 6 are two dimensional histograms of absolute values of residuals versus the expected width W_e, documenting the performance of the correction to the position of clusters assigned to a track, which are distorted by a δ-ray. The odd Figures illustrate the distributions without correction, while the even Figures show the corrected distributions. Data from subsets with fixed observed width of cluster W_o are shown.
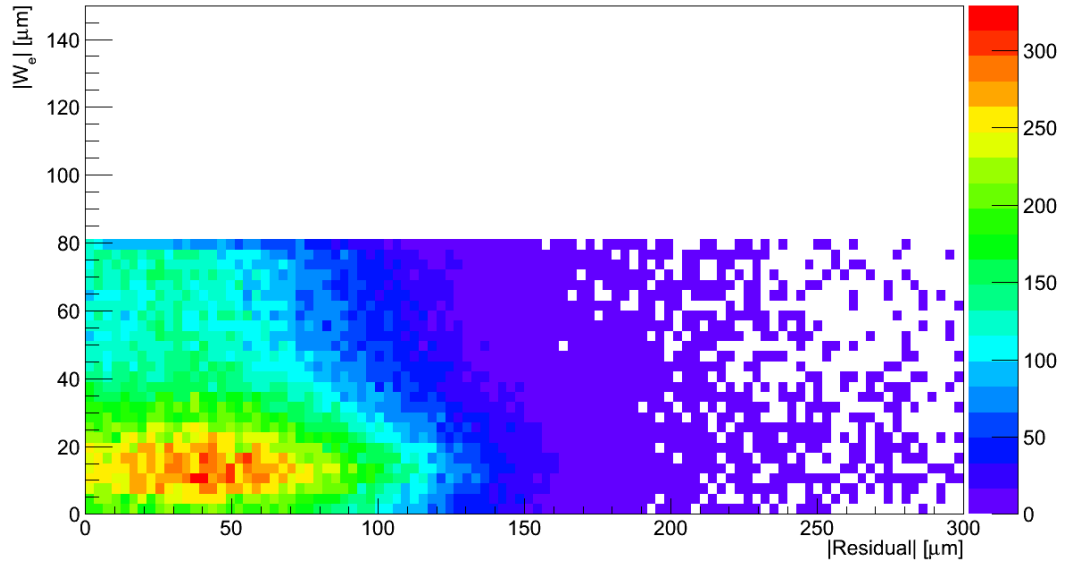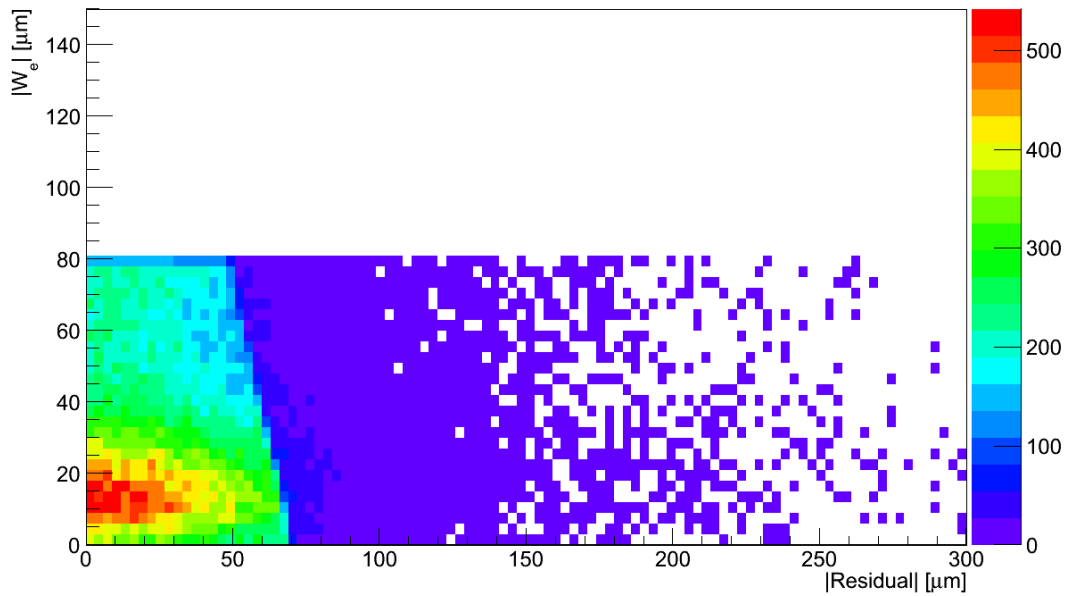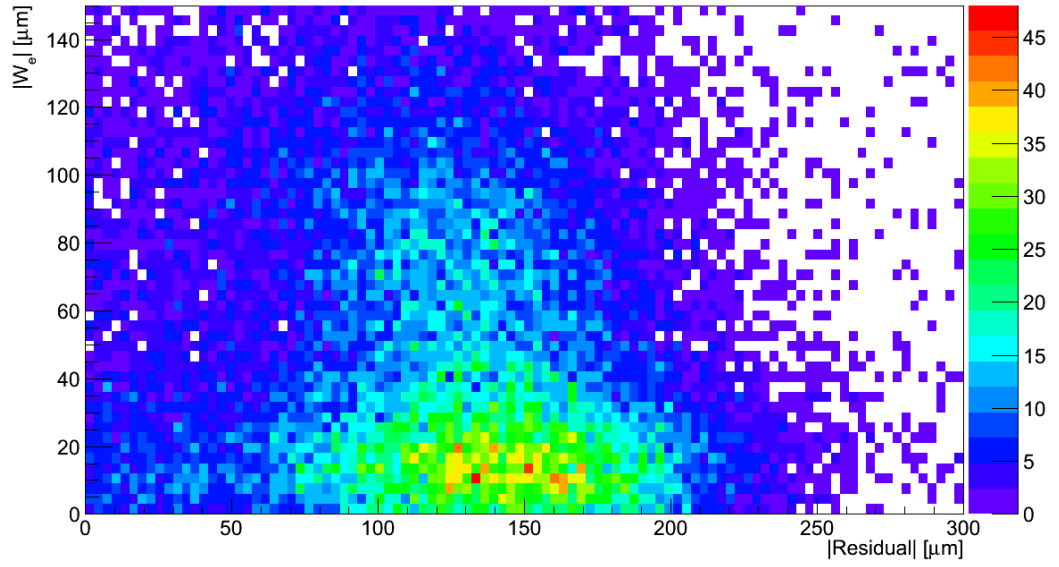
Figure 1: The plot of the absolute value of residuals versus the absolute value of the expected width of the cluster ($W_o = 3$) on a track disturbed by the δ-ray before the correction. The "signal" Gaussian is clearly visible and centred away from zero in residuals.

Figure 2: The plot of the absolute value of residuals versus the absolute value of the expected width of the cluster ($W_o = 3$) on a track disturbed by a δ-ray after the correction. The "signal" Gaussian is clearly visible and centred at zero in residuals.
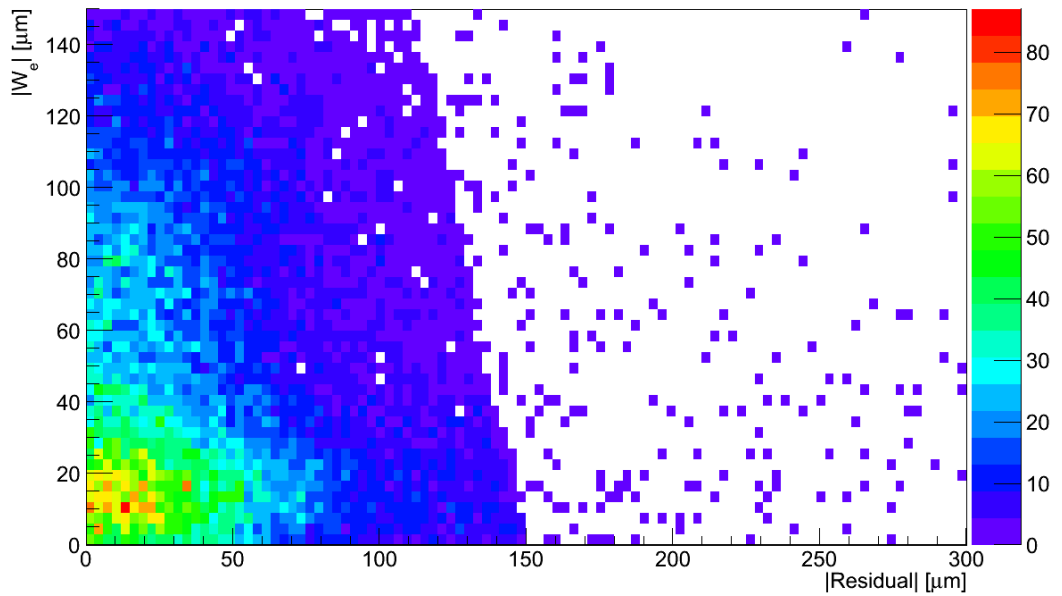
Figure 3: The plot of the absolute value of residuals versus the absolute value of the expected width of the cluster ($W_o = 5$) on a track disturbed by the δ-ray before the correction. The "signal" Gaussian is clearly visible and centred away from zero in residuals.
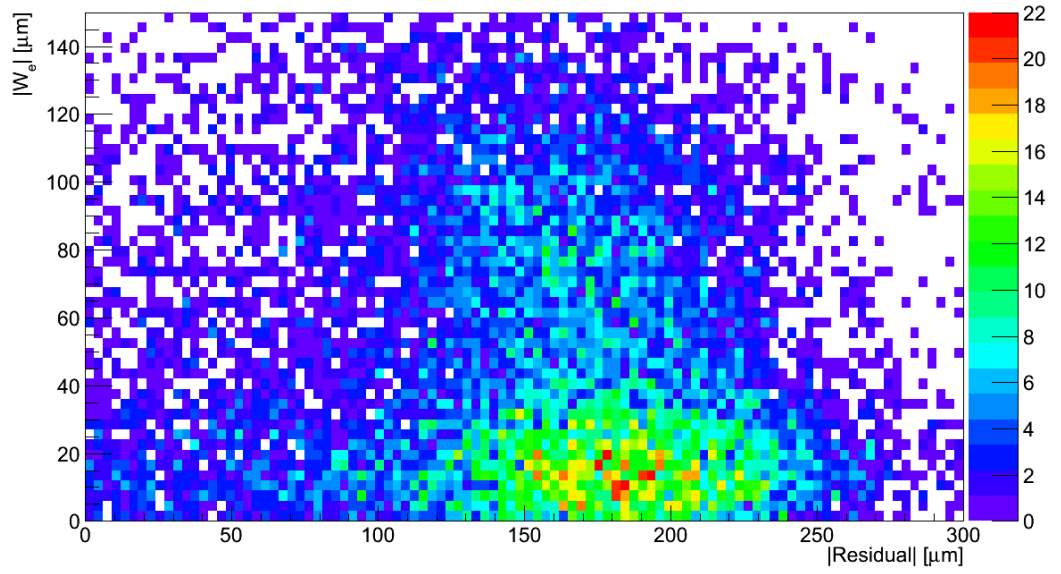

Figure 4: The plot of the absolute value of residuals versus the absolute value of the expected width of the cluster ($W_o = 5$) on a track disturbed by a δ-ray after the correction. The "signal" Gaussian is clearly visible and centred at zero in residuals.

Figure 5: The plot of the absolute value of residuals versus the absolute value of the expected width of the cluster ($W_o = 6$) on a track disturbed by the δ-ray before the correction. The "signal" Gaussian is clearly visible and centred away from zero in residuals.
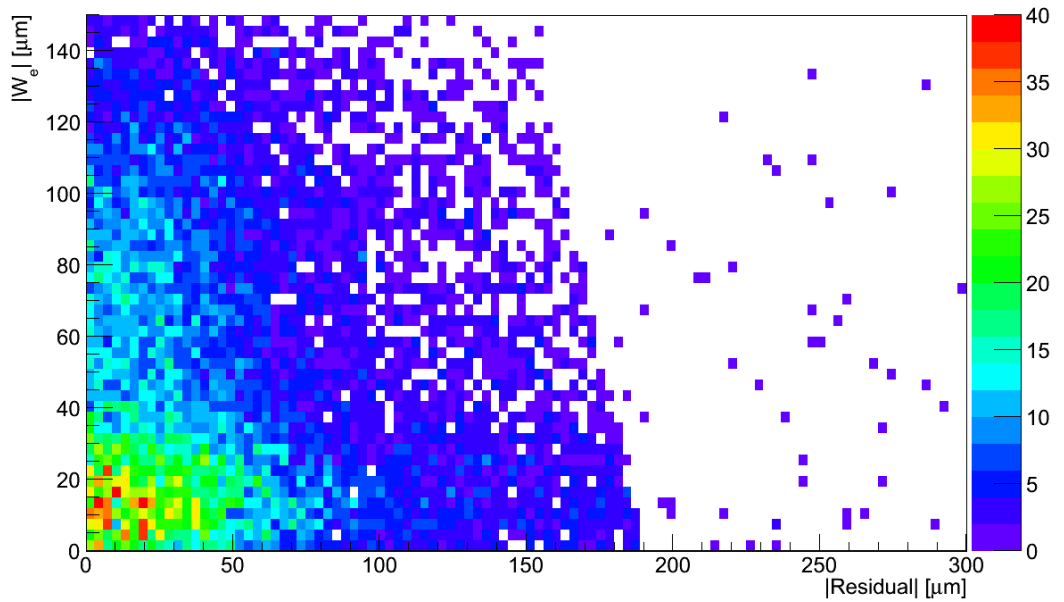

Figure 6: The plot of the absolute value of residuals versus the absolute value of the expected width of the cluster ($W_o = 6$) on a track disturbed by a δ-ray after the correction. The "signal" Gaussian is clearly visible and centred at zero in residuals.